

1 Fitting

1.1 Model: $\Lambda K_S^0, \Lambda K^\pm, \Xi^- K_S^0$

The two-particle relative momentum correlation function may be written theoretically by the Koonin-Pratt equation [?, ?]:

$$C(\mathbf{k}^*) = \int S(\mathbf{r}^*) |\Psi_{\mathbf{k}^*}(\mathbf{r}^*)|^2 d^3 \mathbf{r}^* \quad (1)$$

where $S(\mathbf{r}^*)$ is the pair source distribution, $\Psi_{\mathbf{k}^*}(\mathbf{r}^*)$ is the two-particle wave-function, and k^* is the momentum of one particle in the pair rest frame. In the absence of Coulomb effects, and assuming a spherically Gaussian source of width R , and s-wave scattering, the 1D femtoscopic correlation function can be calculated analytically using:

$$C(k^*) = 1 + C_{QI}(k^*) + C_{FSI}(k^*) \quad (2)$$

C_{QI} describes plane-wave quantum interference:

$$C_{QI}(k^*) = \alpha \exp(-4k^{*2}R^2) \quad (3)$$

where $\alpha = (-1)^{2j}/(2j+1)$ for identical particles with spin j , and $\alpha = 0$ for non-identical particles. For all analyses presented in this note, $\alpha = 0$. C_{FSI} describes the s-wave strong final state interaction between the particles:

$$\begin{aligned} C_{FSI}(k^*) &= (1 + \alpha) \left[\frac{1}{2} \left| \frac{f(k^*)}{R} \right|^2 \left(1 - \frac{d_0}{2\sqrt{\pi}R} \right) + \frac{2\Re f(k^*)}{\sqrt{\pi}R} F_1(2k^*R) - \frac{\Im f(k^*)}{R} F_2(2k^*R) \right] \\ f(k^*) &= \left(\frac{1}{f_0} + \frac{1}{2} d_0 k^{*2} - ik^* \right)^{-1}; \quad F_1(z) = \int_0^z \frac{e^{x^2-z^2}}{z} dx; \quad F_2(z) = \frac{1-e^{-z^2}}{z} \end{aligned} \quad (4)$$

where R is the source size, $f(k^*)$ is the s-wave scattering amplitude, f_0 is the complex scattering length, and d_0 is the effective range of the interaction.

An additional parameter λ is typically included in the femtoscopic fit function to account for the purity of the pair sample. In the case of no residual correlations (to be discussed in Section 1.4), the fit function becomes:

$$C(k^*) = 1 + \lambda [C_{QI}(k^*) + C_{FSI}(k^*)] \quad (5)$$

1.2 Model: $\Xi^- K^\pm$

The two-particle correlation function may be written as:

$$C(\mathbf{k}^*) = \sum_S \rho_S \int S(\mathbf{r}^*) |\Psi_{\mathbf{k}^*}^S(\mathbf{r}^*)|^2 d^3 \mathbf{r}^* \quad (6)$$

where ρ_S is the normalized emission probability of particles in a state with spin S , $S(\mathbf{r}^*)$ is the pair emission source distribution (assumed to be Gaussian), and $\Psi_{\mathbf{k}^*}^S(\mathbf{r}^*)$ is the two-particle wave-function including both strong and Coulomb interactions [?]:

$$\Psi_{\mathbf{k}^*}(\mathbf{r}^*) = e^{i\delta_c} \sqrt{A_c(\eta)} [e^{i\mathbf{k}^* \cdot \mathbf{r}^*} F(-i\eta, 1, i\xi) + f_c(k^*) \frac{\tilde{G}(\rho, \eta)}{r^*}] \quad (7)$$

where $\rho = k^* r^*$, $\eta = (k^* a_c)^{-1}$, $\xi = \mathbf{k}^* \cdot \mathbf{r}^* + k^* r^* \equiv \rho(1 + \cos \theta^*)$, and $a_c = (\mu z_1 z_2 e^2)^{-1}$ is the two-particle Bohr radius (including the sign of the interaction). δ_c is the Coulomb s-wave phase shift, $A_c(\eta)$ is the Coulomb penetration factor, $\tilde{G} = \sqrt{A_c}(G_0 + iF_0)$ is a combination of the regular (F_0) and singular (G_0) s-wave Coulomb functions. $f_c(k^*)$ is the s-wave scattering amplitude:

$$f_c(k^*) = \left[\frac{1}{f_0} + \frac{1}{2} d_0 k^{*2} - \frac{2}{a_c} h(\eta) - ik^* A_c(\eta) \right]^{-1} \quad (8)$$

where, the “h-function”, $h(\eta)$, is expressed through the digamma function, $\psi(z) = \Gamma'(z)/\Gamma(z)$ as:

$$h(\eta) = 0.5[\psi(i\eta) + \psi(-i\eta) - \ln(\eta^2)] \quad (9)$$

In this case, the λ parameter may be included as:

$$C(\mathbf{k}^*) = (1 - \lambda) + \lambda \sum_S \rho_S \int S(\mathbf{r}^*) |\Psi_{\mathbf{k}^*}^S(\mathbf{r}^*)|^2 d^3 \mathbf{r}^* \quad (10)$$

1.3 Momentum Resolution Corrections

Finite track momentum resolution causes the reconstructed momentum of a particle to smear around the true value. This, of course, also holds true for V0 particles. The effect is propagated up to the pairs of interest, which causes the reconstructed relative momentum (k_{Rec}^*) to differ from the true momentum (k_{True}^*). Smearing of the momentum typically will result in a suppression of the signal. More specifically, the smearing will broaden the signal, which would cause a decrease in the extracted radius of the system.

The effect of finite momentum resolution can be investigated using the HIJING MC data, for which both the true and reconstructed momenta are available. Figure 1 shows sample k_{True}^* vs. k_{Rec}^* plots for ΛK^\pm 0-10% analyses; Figure 1a was generated using same-event pairs, while Figure 1b was generated using mixed-event pairs (with $N_{\text{mix}} = 5$).

If there are no contaminations in our particle collection, the plots in Figure 1 should be smeared around $k_{\text{True}}^* = k_{\text{Rec}}^*$; this is mostly true in our analyses. However, there are some interesting features of our results which demonstrate a small (notice the log-scale on the z-axis) contamination in our particle collection. The structure around $k_{\text{Rec}}^* = k_{\text{True}}^* - 0.15 \text{ GeV}/c$ is mainly caused by K_S^0 contamination in our $\Lambda(\bar{\Lambda})$ sample. The remaining structure not distributed about $k_{\text{Rec}}^* = k_{\text{True}}^*$ is due to π and e contamination in our K^\pm sample. These contaminations are more visible in Figure 2, which show k_{Rec}^* vs. k_{True}^* plots (for a small sample of the ΛK^\pm 0-10% central analysis), for which the MC truth (i.e. true, known identity of the particle) was used to eliminate misidentified particles in the $K^+(a)$ and $\Lambda(b)$ collections. (NOTE: This is an old figure and is for a small sample of the data. A new version will be generated shortly. It, nonetheless, demonstrates the point well).

Information gained from looking at k_{Rec}^* vs k_{true} can be used to apply corrections to account for the effects of finite momentum resolution on the correlation functions. A typical method (“Ratio” method) involves using the MC HIJING data to build two correlation functions, $C_{\text{Rec}}(k^*)$ and $C_{\text{True}}(k^*)$, using the generator-level momentum (k_{True}^*) and the measured detector-level momentum (k_{Rec}^*). The data is then corrected by multiplying by the ratio, $C_{\text{True}}/C_{\text{Rec}}$, before fitting. This essentially unsmears the data, which then can be compared directly to theoretical predictions and fits. Although this is conceptually simple, there are a couple of big disadvantages to this method. First, HIJING does not incorporate final-state interactions, so weights must be used when building same-event (numerator) distributions. These weights account for the interactions, and, in the absence of Coulomb interactions, can be calculated using Eq. 2. Of course, these weights are valid only for a particular set of fit parameters. Therefore, in the fitting process, during which the fitter explores a large parameter set, the corrections will not remain valid. As

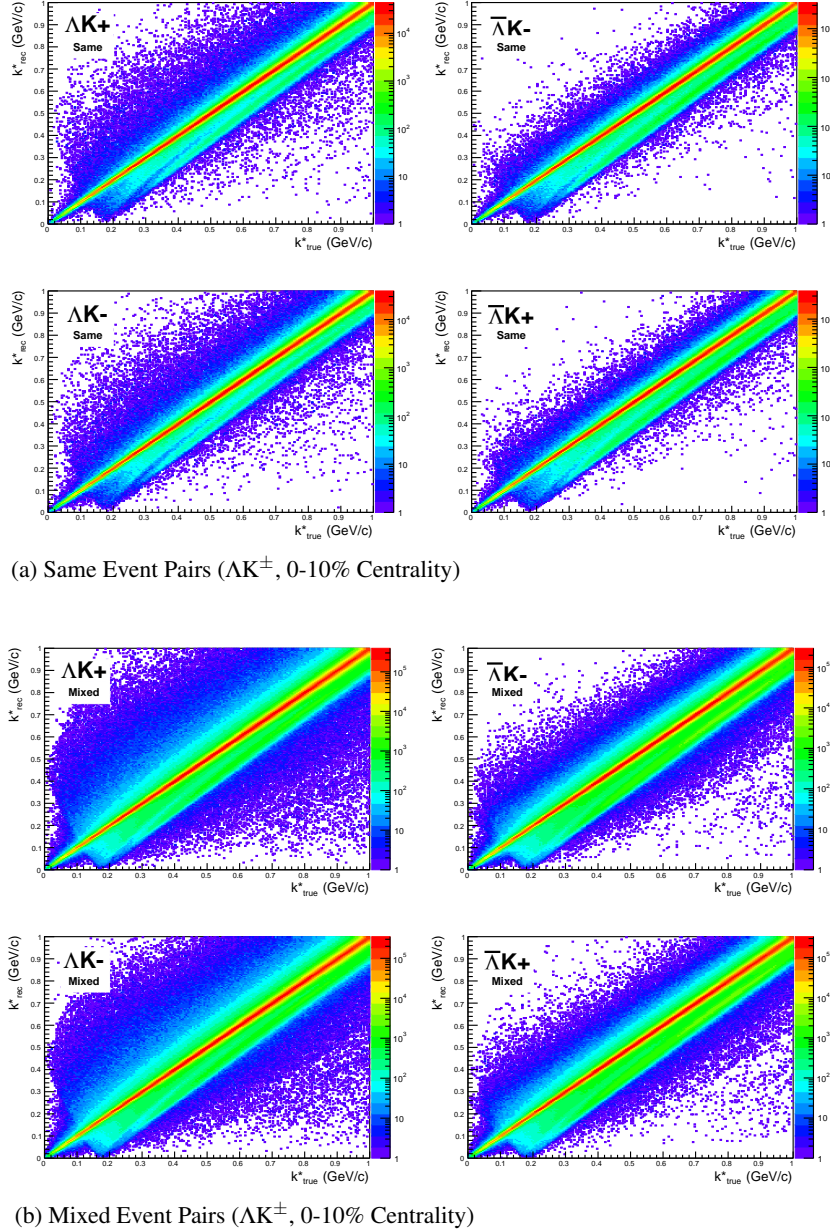
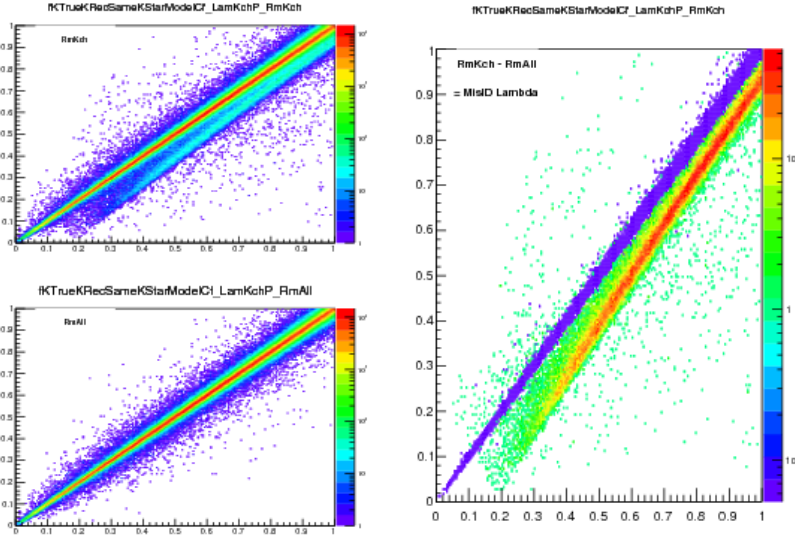
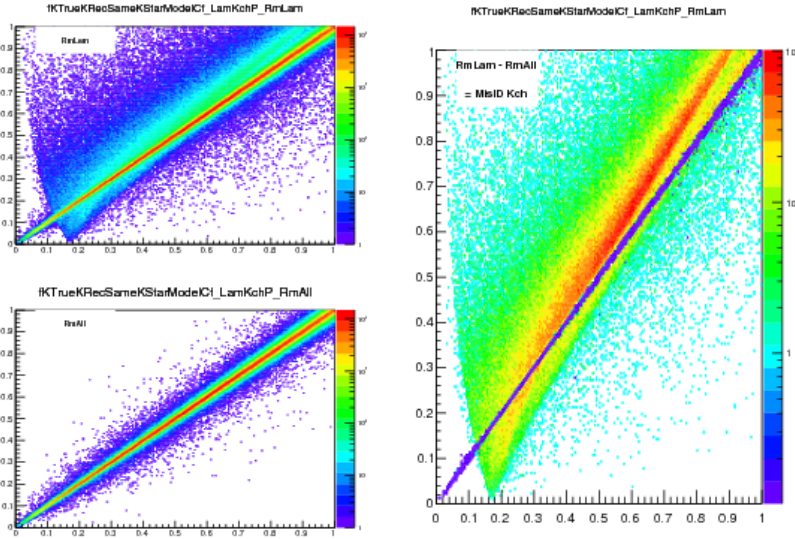


Fig. 1: Sample k_{True}^* vs. k_{Rec}^* plots from MC HIJING events for ΛK^\pm 0-10% analyses. The structure which appears around $k_{\text{Rec}}^* = k_{\text{True}}^* - 0.15 \text{ GeV}/c$ is mainly caused by K_S^0 contamination in our $\Lambda(\bar{\Lambda})$ sample. The remaining structure not distributed about $k_{\text{Rec}}^* = k_{\text{True}}^*$ is due to π and e contamination in our K^\pm sample. These contaminations are more clearly visible in Figure 2

such, applying the momentum resolution correction and fitting becomes a long and drawn out iterative process. An initial parameter set is obtained (through fitting without momentum resolution corrections, theoretical models, or a good guess), then the MC data is analyzed to obtain correlation functions needed to calculate the correction factor, the data is fit using the correction factor, a refined parameter set is extracted, the MC data is analyzed again to obtain the new correction factor, etc. This process continues until the parameter set stabilizes. The second issue concerns statistics. With the MC data available on the grid, we were not able to generate the statistics necessary to use the raw $C_{\text{True}}/C_{\text{Rec}}$ ratio. The ratio was not stable, and when applied to the data, obscured the signal. Attempting to fit the ratio to use to generate the corrections also proved problematic. However, as HIJING does not include final-state interactions, the same-event and mixed-event pairs are very similar (with the exception of things like



(a) (Top Left) All misidentified K^+ excluded. (Bottom Left) All misidentified Λ and K^+ excluded. (Right) The difference of (Top Left) - (Bottom Left), which reveals the contamination in our Λ collection. The structure which appears around $k_{\text{Rec}}^* = k_{\text{True}}^* - 0.15 \text{ GeV}/c$ is mainly caused by K_S^0 contamination in our $\Lambda(\bar{\Lambda})$ sample.



(b) (Top Left) All misidentified Λ excluded. (Bottom Left) All misidentified Λ and K^+ excluded. (Right) The difference of (Top Left) - (Bottom Left), which reveals the contamination in our K^+ collection. The structure not distributed about $k_{\text{Rec}}^* = k_{\text{True}}^*$ is due to π and e^- contamination in our K^\pm sample.

Fig. 2: In the figure, the y-axis = k_{Rec}^* , and the x-axis = k_{True}^* . (Left) k_{Rec}^* vs. k_{True}^* plots for a small sample of the ΛK^+ 0-10% central analysis, MC truth was used to eliminate misidentified particles in the K^+ (a) and Λ (b) collections. (Right) The difference of the top left and bottom left plots. Contaminations in our particle collections are clearly visible. Figure (a) demonstrates a K_S^0 contamination in our Λ collection; Figure (b) demonstrates a π and e^- contamination in our K^\pm collection.

energy and momentum conservation, etc). Therefore, one may build the numerator distribution using mixed-event pairs. This corresponds, more or less, to simply running the weight generator through the detector framework.

A second approach (“Matrix” method) is to use information gained from plots like those in Figure 1,

which can be considered response matrices. The response matrix describes quantitatively how each k_{Rec}^* bin receives contributions from multiple k_{True}^* bins, and can be used to account for the effects of finite momentum resolution. With this approach, the resolution correction is applied on-the-fly during the fitting process by propagating the theoretical correlation function (fit) through the response matrix, according to:

$$C_{\text{Fit}}(k_{\text{Rec}}^*) = \frac{\sum_{k_{\text{True}}^*} M_{k_{\text{Rec}}^*, k_{\text{True}}^*} C_{\text{Fit}}(k_{\text{True}}^*)}{\sum_{k_{\text{True}}^*} M_{k_{\text{Rec}}^*, k_{\text{True}}^*}} \quad (11)$$

where $M_{k_{\text{Rec}}^*, k_{\text{True}}^*}$ is the response matrix (Figure 1), $C_{\text{Fit}}(k_{\text{True}}^*)$ is the fit binned in k_{True}^* , and the denominator normalizes the result.

Equation 11 describes that, for a given k_{Rec}^* bin, the observed value of $C(k_{\text{Rec}}^*)$ is a weighted average of all $C(k_{\text{True}}^*)$ values, where the weights are the normalized number of counts in the $[k_{\text{Rec}}^*, k_{\text{True}}^*]$ bin. As seen in Figure 1, overwhelmingly the main contributions comes from the $k_{\text{Rec}}^* = k_{\text{True}}^*$ bins. Although the correction is small, it is non-negligible for the low- k^* region of the correlation function.

Here, the momentum resolution correction is applied to the fit, not the data. In other words, during fitting, the theoretical correlation function is smeared just as real data would be, instead of unsmearing the data. This may not be ideal for the theorist attempting to compare a model to experimental data, but it leaves the experimental data unadulterated. The current analyses use this second approach to applying momentum resolution corrections because of two major advantages. First, the MC data must be analyzed only once, and no assumptions about the fit are needed. Secondly, the momentum resolution correction is applied on-the-fly by the fitter, delegating the iterative process to a computer instead of the user.

The two methods described above, Ratio and Matrix, should reproduce the same results at the parameter set used to generate the $C_{\text{True}}/C_{\text{Rec}}$ needed for the Ratio method. Figure 3 shows that the two methods converge as the binning size is decreased.

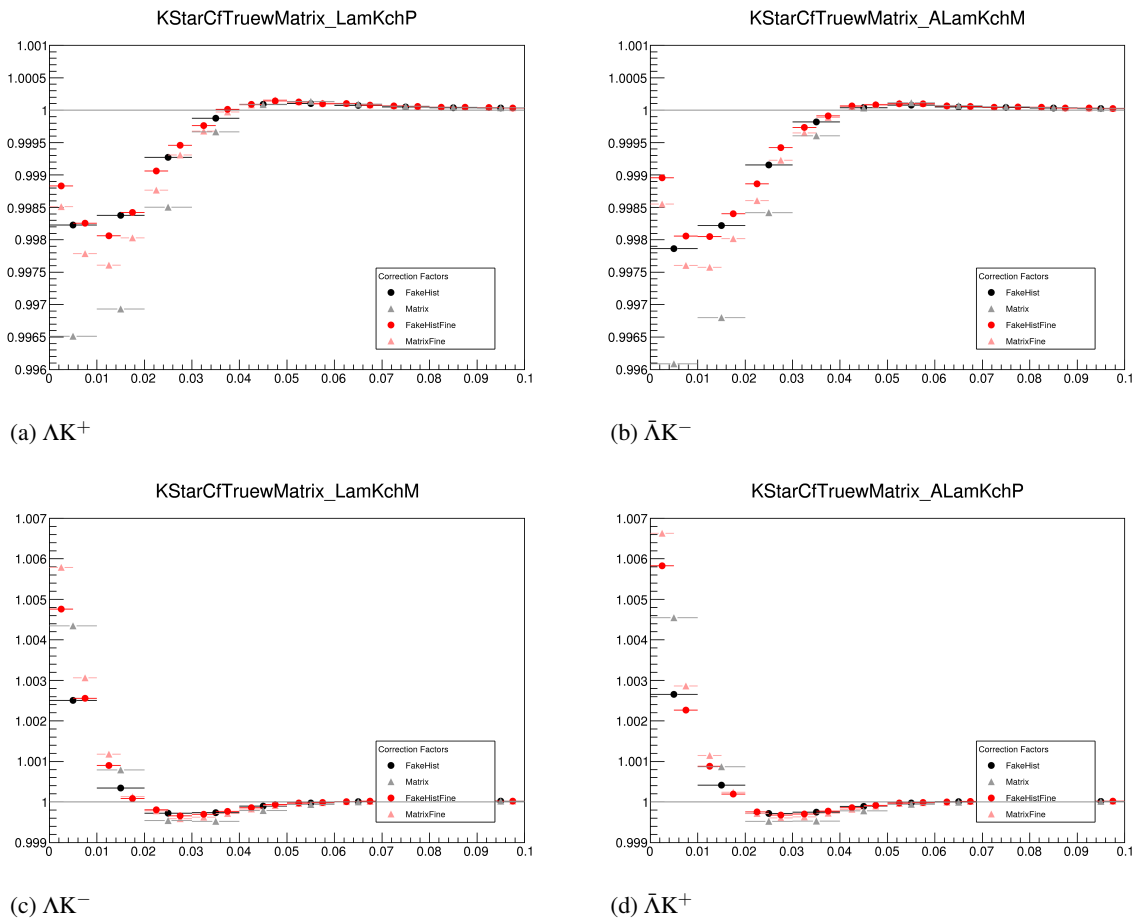


Fig. 3: Comparison of the two methods, Ratio and Matrix, for accounting for momentum resolution effects with HIJING. The Ratio method corresponds to the “FakeHist” histograms (circles), while the Matrix method corresponds to the “Matrix” histograms (triangles). Black shows a coarse binning, while red shows a finer binning.

1.4 Residual Correlations

The purpose of this analysis is to study both the interaction, and the scale of the emitting source, of the pairs. In order to obtain correct results, it is important for our particle collections to consist of primary particles. In practice, this is difficult to achieve for our Λ and $\bar{\Lambda}$ collections. Many of our Λ particles are not primary, but originate as decay products from other hyperons, including Σ^0 , Ξ^0 , Ξ^- and $\Sigma^{*(+,-,0)}(1385)$. Additionally, many of our K particles are not primary, but decay from $K^{*(+,-,0)}(892)$ parents. In these decays, the daughter Λ or K_S^0 carries away a momentum very similar to that of its parent. As a result, the correlation function between a secondary Λ and, for instance, a K^+ will be sensitive to, and dependent upon, the interaction between the parent of the Λ and the K^+ . In effect, the correlation between the parent of the Λ and the K^+ (ex. $\Sigma^0 K^+$) will be visible, although smeared out, in the ΛK^+ data; we call this a residual correlation resulting from feed-down. The contributions from the primary correlation, residual correlations, and fake pairs on the finally measure data is shown schematically in Figure 4. Residual correlations are important in an analysis when three criteria are met [?]: i) the parent correlation signal is large, ii) a large fraction of pairs in the sample originate from the particular parent system, and iii) the decay momenta are comparable to the expected correlation width in k^* .

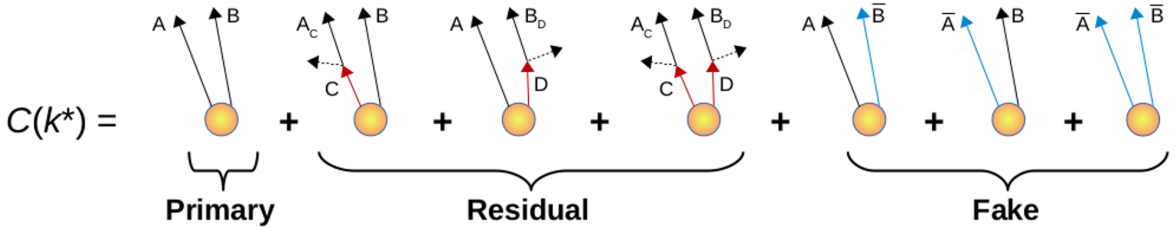


Fig. 4: A schematic representation of the contributions to the finally measured data from the primary correlation, residual correlations, and fake pairs.

As it is difficult for us to eliminate these residual correlations in our analyses, we must attempt to account for them in our fit. To achieve this, we will simultaneously fit the data for both the primary correlation function and the residual correlations. For example, in the simple case of a ΛK^+ analysis with residuals arising solely from $\Sigma^0 K^+$ feed-down:

$$C_{measured}(k_{\Lambda K^+}^*) = 1 + \lambda_{\Lambda K^+}[C_{\Lambda K^+}(k_{\Lambda K^+}^*) - 1] + \lambda_{\Sigma^0 K^+}[C_{\Sigma^0 K^+}(k_{\Lambda K^+}^*) - 1]$$

$$C_{\Sigma^0 K^+}(k_{\Lambda K^+}^*) \equiv \frac{\sum_{k_{\Sigma^0 K^+}^*} C_{\Sigma^0 K^+}(k_{\Sigma^0 K^+}^*) T(k_{\Sigma^0 K^+}^*, k_{\Lambda K^+}^*)}{\sum_{k_{\Sigma^0 K^+}^*} T(k_{\Sigma^0 K^+}^*, k_{\Lambda K^+}^*)} \quad (12)$$

$C_{\Sigma^0 K^+}(k_{\Sigma^0 K^+}^*)$ is the $\Sigma^0 K^+$ correlation function from, for instance, Equation 2, and T is the transform matrix generated with THERMINATOR. The transform matrix is formed for a given parent pair, AB, by taking all ΛK pairs originating from AB, calculating the relative momentum of the parents (k_{AB}^*) and daughters ($k_{\Lambda K}^*$), and filling a two-dimensional histogram with the values. The transform matrix is essentially an unnormalized probability distribution mapping the k^* of the parent pair to that of the daughter pair when one or both parents decay. An example of such transform matrices can be found in Figures 5 and 6.

The above equation can be easily extended to include feed-down from more sources:

$$\begin{aligned}
C_{measured}(k_{\Lambda K}^*) &= 1 + \lambda_{\Lambda K}[C_{\Lambda K}(k_{\Lambda K}^*) - 1] + \lambda_{\Sigma^0 K}[C_{\Sigma^0 K}(k_{\Lambda K}^*) - 1] + \dots \\
&\quad + \lambda_{P_1 P_2}[C_{P_1 P_2}(k_{\Lambda K}^*) - 1] + \lambda_{other}[C_{other}(k_{\Lambda K}^*) - 1]
\end{aligned}
\tag{13}$$

$$C_{P_1 P_2}(k_{\Lambda K}^*) \equiv \frac{\sum_{k_{P_1 P_2}^*} C_{P_1 P_2}(k_{P_1 P_2}^*) T(k_{P_1 P_2}^*, k_{\Lambda K}^*)}{\sum_{k_{P_1 P_2}^*} T(k_{P_1 P_2}^*, k_{\Lambda K}^*)}$$

Or, more compactly:

$$C_{measured}(k_{\Lambda K}^*) = 1 + \sum_i \lambda_i [C_i(k_{\Lambda K}^*) - 1] \tag{14}$$

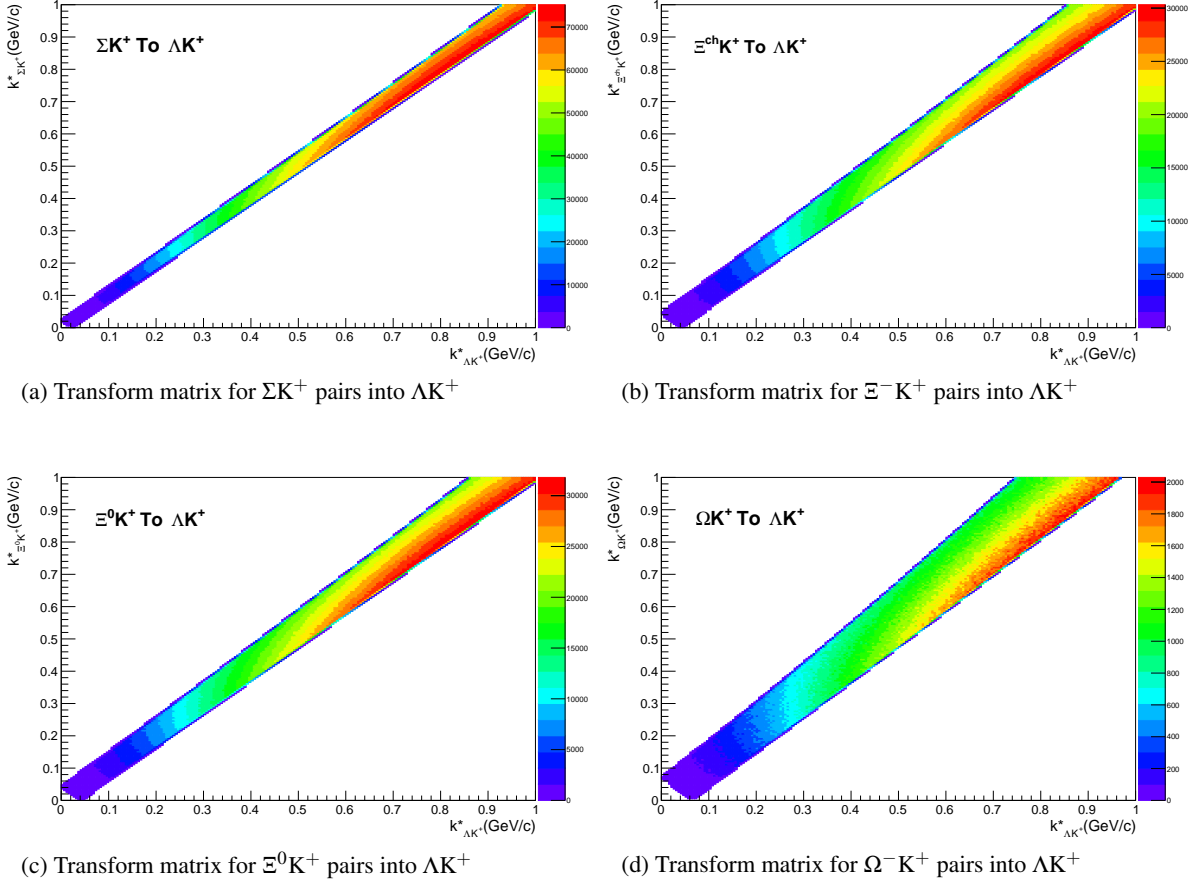


Fig. 5: Sample Transform Matrices generated with THERMINATOR for ΛK^+ Analysis

So, in practice, we model the correlation function of the parents (ex. $\Sigma^0 K^+$), and run the correlation function through the appropriate transform matrix to determine the contribution to the daughter correlation function (ex. ΛK^+). A few questions still remain. First, what λ values should be used in the above equation? One option would be to leave all of these λ -parameters free during the fit process. However, this would introduce a huge number of new parameters into the fitter, and would make the fit results less trustworthy. The λ parameters roughly dictate the strength of the parent contribution to the daughter pair. Additionally, as found in [?], the reconstruction efficiency for primary Λ particles is nearly equal to that of Λ particles originating from Σ , Σ^* , Ξ^0 , Ξ^- , and Ω hyperons. Therefore, the λ parameter for

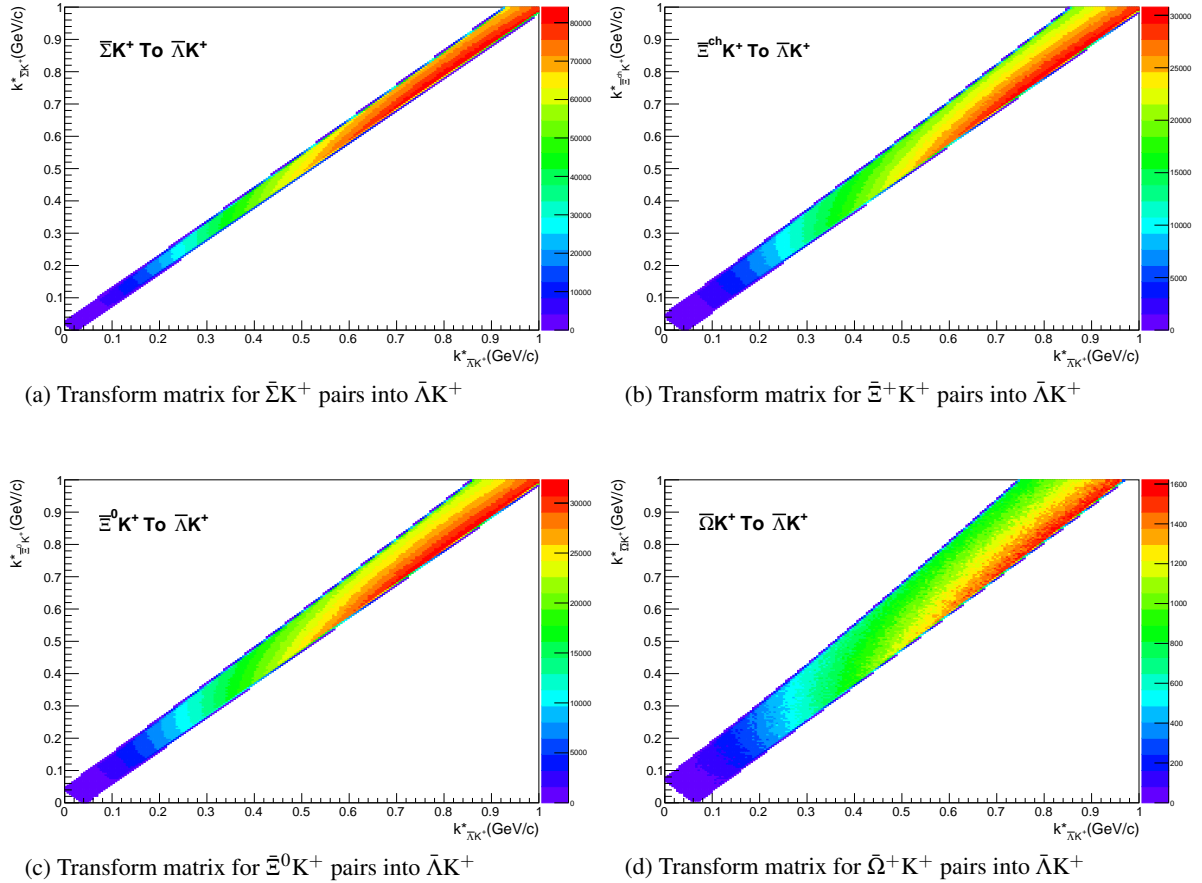


Fig. 6: Sample Transform Matrices generated with THERMINATOR for $\bar{\Lambda}K^+$ Analysis

parent system AB can be estimated using THERMINATOR as the total number of ΛK pairs originating from AB (N_{AB}) divided by the total number of ΛK pairs (N_{Total}):

$$\lambda_{AB} = \frac{N_{AB}}{N_{Total}} \quad (15)$$

Note, for our study, we consider a particle to be primary if its parent has a proper decay length of < 4 fm. The λ values used can be found in Table 1, for the case of both three and ten residual contributors. In the table, we also list the λ values used for “Other” and “Fakes”. The “Other” category contains pairs which are not primary, and which do not originate from the (3 or 10) residual pairs included in the fit. The “Fakes” category represents pairs that are mistakenly identified as ΛK . To estimate this λ_{Fakes} value, we assumed that the number of fake pairs was equal to the total number of pairs multiplied by the Λ purity (i.e. assuming perfect purity for the kaons); or, more simply, $\lambda_{Fakes} = 1.0 - \text{Purity}(\Lambda)$. For both of these contributors (“Other” and “Fakes”), we assume that these correlations average to unity, and therefore do not contribute to the final correlation function.

ΛK^+ residuals		$\bar{\Lambda}K^-$ residuals		ΛK^- residuals		$\bar{\Lambda}K^+$ residuals		ΛK_S^0 residuals		$\bar{\Lambda}K_S^0$ residuals	
Pair System	λ value	Pair System	λ value	Pair System	λ value	Pair System	λ value	Pair System	λ value	Pair System	λ value
3 Residuals											
ΛK^+	0.488	$\bar{\Lambda}K^-$	0.488	ΛK^-	0.487	$\bar{\Lambda}K^+$	0.489	ΛK_S^0	0.505	$\bar{\Lambda}K_S^0$	0.507
$\Sigma^0 K^+$	0.103	$\bar{\Sigma}^0 K^-$	0.102	$\Sigma^0 K^-$	0.102	$\bar{\Sigma}^0 K^+$	0.102	$\Sigma^0 K_S^0$	0.112	$\bar{\Sigma}^0 K_S^0$	0.111
$\Xi^0 K^+$	0.046	$\bar{\Xi}^0 K^-$	0.040	$\Xi^0 K^-$	0.046	$\bar{\Xi}^0 K^+$	0.041	$\Xi^0 K_S^0$	0.050	$\bar{\Xi}^0 K_S^0$	0.044
$\Xi^- K^+$	0.063	$\bar{\Xi}^+ K^-$	0.056	$\Xi^- K^-$	0.062	$\bar{\Xi}^+ K^+$	0.057	$\Xi^- K_S^0$	0.068	$\bar{\Xi}^+ K_S^0$	0.062
Other	0.252	Other	0.261	Other	0.255	Other	0.259	Other	0.217	Other	0.222
Fakes	0.048	Fakes	0.048	Fakes	0.048	Fakes	0.048	Fakes	0.048	Fakes	0.048
10 Residuals											
ΛK^+	0.317	$\bar{\Lambda}K^-$	0.319	ΛK^-	0.317	$\bar{\Lambda}K^+$	0.318	ΛK_S^0	0.342	$\bar{\Lambda}K_S^0$	0.344
$\Sigma^0 K^+$	0.105	$\bar{\Sigma}^0 K^-$	0.105	$\Sigma^0 K^-$	0.104	$\bar{\Sigma}^0 K^+$	0.106	$\Sigma^0 K_S^0$	0.113	$\bar{\Sigma}^0 K_S^0$	0.114
$\Xi^0 K^+$	0.047	$\bar{\Xi}^0 K^-$	0.042	$\Xi^0 K^-$	0.047	$\bar{\Xi}^0 K^+$	0.042	$\Xi^0 K_S^0$	0.051	$\bar{\Xi}^0 K_S^0$	0.045
$\Xi^- K^+$	0.064	$\bar{\Xi}^+ K^-$	0.058	$\Xi^- K^-$	0.063	$\bar{\Xi}^+ K^+$	0.059	$\Xi^- K_S^0$	0.069	$\bar{\Xi}^+ K_S^0$	0.063
$\Sigma^{*+} K^+$	0.049	$\bar{\Sigma}^{*-} K^-$	0.047	$\Sigma^{*+} K^-$	0.048	$\bar{\Sigma}^{*-} K^+$	0.048	$\Sigma^{*+} K_S^0$	0.052	$\bar{\Sigma}^{*-} K_S^0$	0.051
$\Sigma^{*-} K^+$	0.044	$\bar{\Sigma}^{*+} K^-$	0.046	$\Sigma^{*-} K^-$	0.044	$\bar{\Sigma}^{*+} K^+$	0.047	$\Sigma^{*-} K_S^0$	0.047	$\bar{\Sigma}^{*+} K_S^0$	0.050
$\Sigma^{*0} K^+$	0.044	$\bar{\Sigma}^{*0} K^-$	0.041	$\Sigma^{*0} K^-$	0.044	$\bar{\Sigma}^{*0} K^+$	0.042	$\Sigma^{*0} K_S^0$	0.047	$\bar{\Sigma}^{*0} K_S^0$	0.045
ΛK^{*0}	0.041	$\bar{\Lambda}K^{*0}$	0.042	$\Lambda \bar{K}^{*0}$	0.041	$\bar{\Lambda}K^{*0}$	0.042	ΛK^{*0}	0.020	$\bar{\Lambda}K^{*0}$	0.020
$\Sigma^0 K^{*0}$	0.037	$\bar{\Sigma}^0 \bar{K}^{*0}$	0.037	$\Sigma^0 \bar{K}^{*0}$	0.037	$\bar{\Sigma}^0 K^{*0}$	0.037	$\Sigma^0 K^{*0}$	0.017	$\bar{\Sigma}^0 K^{*0}$	0.018
$\Xi^0 K^{*0}$	0.017	$\bar{\Xi}^0 \bar{K}^{*0}$	0.015	$\Xi^0 \bar{K}^{*0}$	0.017	$\bar{\Xi}^0 K^{*0}$	0.015	$\Xi^0 K^{*0}$	0.008	$\bar{\Xi}^0 K^{*0}$	0.007
$\Xi^- K^{*0}$	0.022	$\bar{\Xi}^+ \bar{K}^{*0}$	0.021	$\Xi^- \bar{K}^{*0}$	0.022	$\bar{\Xi}^+ K^{*0}$	0.021	$\Xi^- K^{*0}$	0.011	$\bar{\Xi}^+ K^{*0}$	0.010
Other	0.166	Other	0.174	Other	0.169	Other	0.171	Other	0.176	Other	0.181
Fakes	0.048	Fakes	0.048	Fakes	0.048	Fakes	0.048	Fakes	0.048	Fakes	0.048

Table 1: λ values for the individual components of the ΛK correlation functions for the case of 3 and 10 residual contributions.

Now, the remaining question is how do we model the parent correlation functions? In an ideal world, we would simply look up the parent interaction in some table, and input this into our Lednicky equation (for the case of one or more charge neutral particle in the pair), or run it through the CoulombFitter machinery described in Sec.1.2. Unfortunately, the world in which we live is not perfect, such a table does not exists, and little is known about the interaction between the residual pairs in this study. One solution would be to introduce a set of scattering parameters and radii for each residual system. However, as was the case of the λ -parameters above, this would introduce a large number of additional fit parameters, and would make our fitter too unconstrained and would yield untrustworthy results. The second option, which is adopted in this analysis, is to assume all residual pairs have the same source size as the daughter pair, and all Coulomb-neutral residual pairs also share the same scattering parameters as the daughter pair (the case of charged pairs, such as $\Xi^- K^\pm$ or $\Sigma^{*\pm} K^\pm$, will be described below).

Concerning the radii of the residual parent pairs, it was suggested that these should be set to smaller values than those of the daughter pair. In the interest of minimizing the number of parameters in the fitter, we tested this by introducing an m_T -scaling of the parents' radii. The motivation for this scaling comes from the approximate m_T -scaling of the radii observed in ???. To achieve this scaling, we assume the radii follow an inverse-square-root distribution: $R_{AB} = \alpha m_T^{-1/2}$. Then, it follows that we should scale the parent radii as:

$$R_{AB} = R_{\Lambda K} \left(\frac{m_{T,AB}}{m_{T,\Lambda K}} \right)^{-1/2} \quad (16)$$

The values of m_T for each pair system were taken from THERMINATOR. As the fitter dances around parameter space and selects a new radius for the ΛK system, the radii of the residuals is simply the ΛK radius scaled by the appropriate factor, given above (Eq.16). In the end, this scaling factor made no significant difference in our fit results, so this complication is excluded from our final results. Note that this is not surprising, as the most extreme scaling factor was, in the case of using 10 residual systems, between ΛK with $m_{T,\Lambda K} \approx 1.4 \text{ GeV}/c^2$ and $\Xi^- K^{*0}$ with $m_{T,\Xi^- K^{*0}} \approx 1.8 \text{ GeV}/c^2$, resulting in a scale factor of ≈ 0.9 .

Now, as hinted above, accounting for charged residuals adds a complication in that they necessitate the inclusion of the CoulombFitter (described in Sec. 1.7) into the process. The complication of combining the two fitters is not troubling; however, the substantial increase in the fitting time is (the parallelization of the CoulombFitter across a large number of GPU cores, to drastically decrease run-time, is currently underway). We have two solutions to bypass such a large increase in run time. First, we can use our experimental $\Xi^{ch} K^{ch}$ data to represent all charged parent pair system. In this case, there is no need to make any assumption about scattering parameters or source sizes, as we already have the experimental data. The downside is that, especially in the 30-50% centrality bin, the statistics are low and error bars large. Alternatively, we can assume the strong interaction is negligible in the charged residual, and generate the parent correlation function given radius and λ parameters. We find in our $\Xi^{ch} K^{ch}$ study that a Coulomb-only description of the system describes, reasonably well, the broad features of the correlation. The strong interaction is necessary for the fine details. However, as these correlations are run through a transform matrix, which largely flattens out and fine details, a Coulomb-only description should be sufficient. In practice, this Coulomb-only scenario is achieved by first building a large number of Coulomb-only correlations for various radii and λ parameter values, and interpolating from this grid during the fitting process. We find consistent results between using the ΞK data and the Coulomb-only interpolation method. When quantifying the $\Xi^- K^\pm$ residual contribution, the experimental $\Xi^- K^\pm$ data is always used. When the number of residual pairs used is increased to 10, so that contributors such as $\Sigma^{*+} K^-$ enter the picture, the Coulomb-only interpolation method is used. In other words, the ΞK experimental data is only used to model the ΞK residual contribution, all other charged pairs are treated with the Coulomb-only interpolation method.

Two examples of how very different transform matrices can alter a correlation function are shown in Figures 7 and 8 below. These figures were taken using parameter values obtained from fits to the data. In the top left corner of the figures, the input correlation function (closed symbols) is shown together with the output, transformed, correlation function (open symbols). In the bottom left, the transformed correlation is shown by itself (with zoomed y-axis). This is especially helpful when the λ parameter is very small, in which case the contribution in the top left can look flat, but the zoomed in view in the bottom left shows the structure. The right two plots in each figure show the transform matrix without (top right) and with (bottom right) a log-scale on the z-axis. Note, more examples of these transforms can be found in Sec. ??.

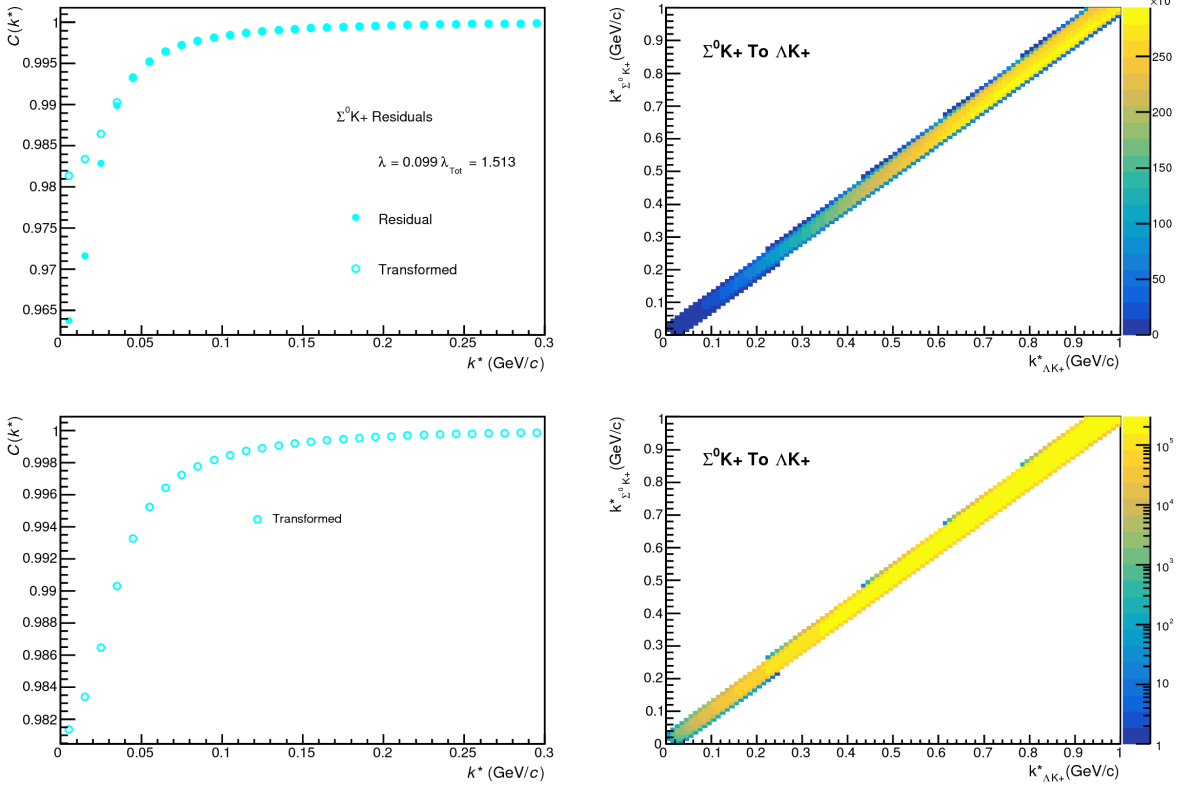


Fig. 7: $\Sigma^0 K^+$ Transform. These figures were taken using parameter values obtained from fits to the data. In the top left corner of the figures, the input correlation function (closed symbols) is shown together with the output, transformed, correlation function (open symbols). In the bottom left, the transformed correlation is shown by itself. The right two plots in each figure show the transform matrix without (top right) and with (bottom right) a log-scale on the z-axis.

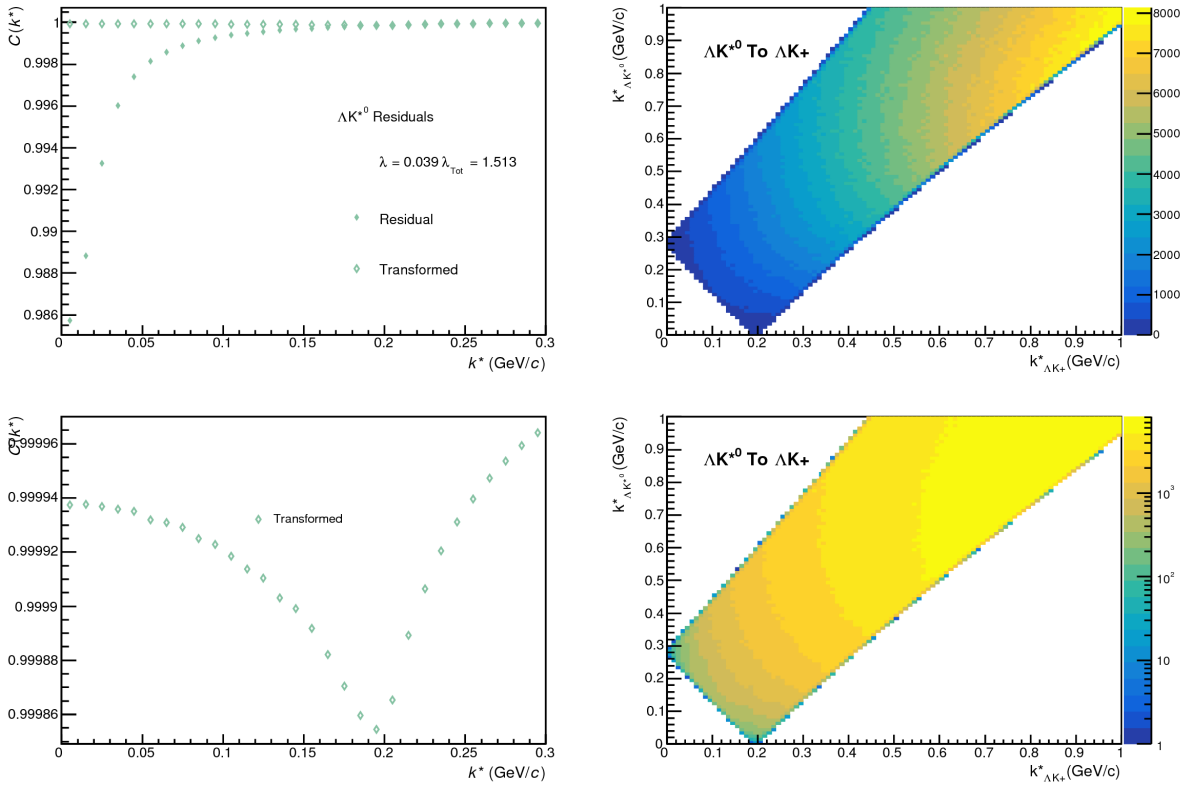


Fig. 8: ΔK^{*0} Transform. These figures were taken using parameter values obtained from fits to the data. In the top left corner of the figures, the input correlation function (closed symbols) is shown together with the output, transformed, correlation function (open symbols). In the bottom left, the transformed correlation is shown by itself. The right two plots in each figure show the transform matrix without (top right) and with (bottom right) a log-scale on the z-axis.

1.5 Non-Flat Background

We observe a significant non-femtoscopic, non-flat, background in all of our correlations at large k^* . This background increases with decreasing centrality, is the same amongst all ΛK^\pm pairs, and is more pronounced in the ΛK_S^0 system, as can be seen in Fig. 9. Figure 10a shows that THERMINATOR 2 simulation does a good job of describing the difference in backgrounds between ΛK^\pm and ΛK_S^0 .

Before beginning, it is important to note that the difference in ΛK^\pm and ΛK_S^0 backgrounds is due mainly to the difference in kinematic cuts, not due to any interesting physics. Figure 10b shows that, for THERMINATOR simulation, when restrictions are imposed on the p_T of the K_S^0 to more closely match the K^\pm cuts, the backgrounds align much better. Therefore, we conclude that the difference in background between ΛK^\pm and ΛK_S^0 observed in our experimental data is simply due to a difference in kinematic cuts between K^\pm and K_S^0 particles.

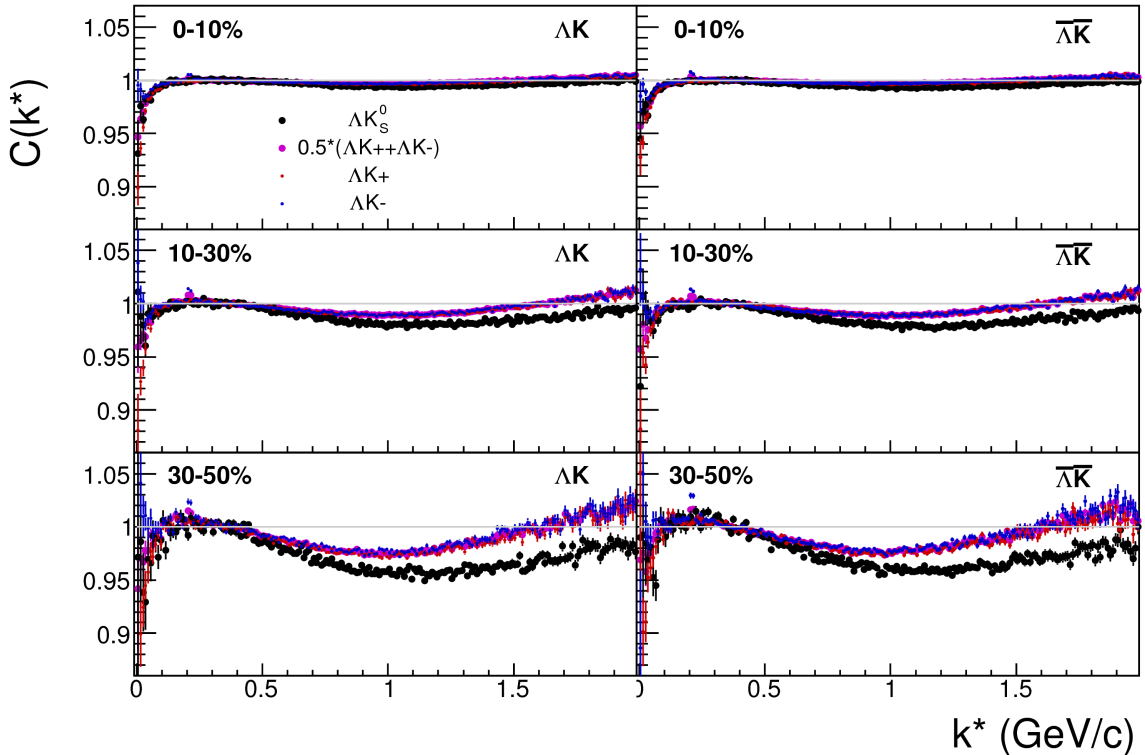


Fig. 9: A comparison on the non-femtoscopic backgrounds observed in our ΛK experimental data.

It is suggested that this background effect is due primarily to particle collimation associated with elliptic flow [?]. More specifically, these backgrounds result from mixing events with unlike event-plane angles (Ψ_{EP}). As explained in [?], when elliptic flow is present, all particles are more likely to be emitted in a specific direction (in-plane), as opposed to a perpendicular direction. Therefore, the difference in momenta for pairs of particles tends to be smaller, compared to the case of no flow. In the case of mixed-event pairs, the two events used do not share an event-plane, and therefore there is no collimation effect in the pairs from flow. As a result, pairs with larger momentum are more likely when mixed-events are used, causing the correlation function to be observed below unity. In general, a dip below unity, at a given k^* , means it is more probable to find a pair at that k^* when the daughters are taken from mixed-events, as compared to when they are taken from the same event.

This same reasoning suggests that the background should lead to an enhancement at low- k^* . The enhancement at high- k^* ($k^* \gtrsim 1.5$ GeV/c) does not result from the collective flow of the system. We are not

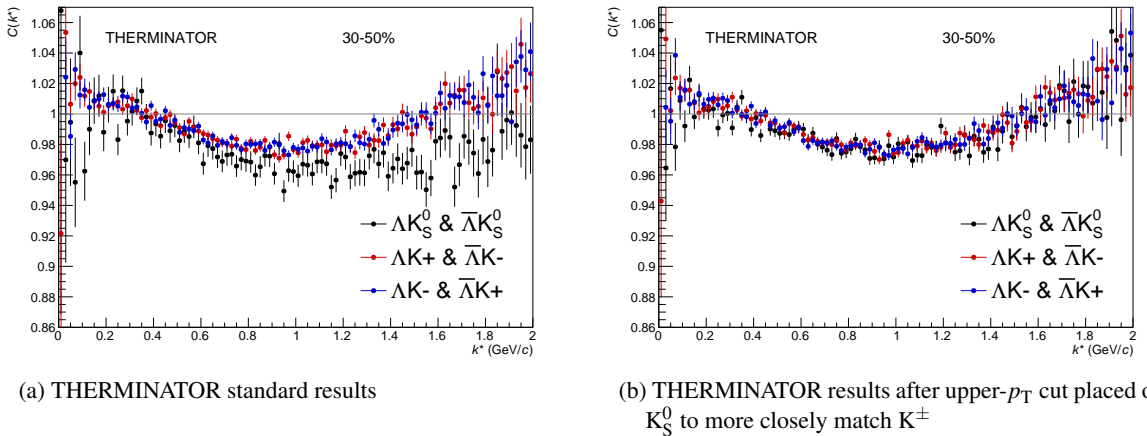


Fig. 10: THERMINATOR 2 simulation for ΛK^+ (red), ΛK^- (blue), and ΛK_S^0 (black). In 10a, we show the standard THERMINATOR 2 results. THERMINATOR 2 does a good job describing qualitatively the different between the ΛK^\pm and ΛK_S^0 backgrounds. In 10b, an upper- p_T cut was placed on the K_S^0 particles to more closely match the K^\pm kinematic cuts. After this tweak, the ΛK^\pm and ΛK_S^0 backgrounds agree much better.

certain was causes this enhancement, but typical suspects are jet-like correlations and resonance decays.

We can split our correlation functions into three main regions. First, the low- k^* region ($k^* \lesssim 0.3$ GeV/c) contains the femtoscopic correlations, as well as a likely enhancement from the background. The intermediate- k^* region ($0.3 \lesssim k^* \gtrsim 1.5$ GeV/c) contains a suppression from the background. Finally, the high- k^* region ($k^* \gtrsim 1.5$ GeV/c) contains an enhancement with unknown origin.

THERMINATOR 2 simulation has been shown to reproduce the background features in a πK analysis [?]. As the background effect can be attributed mainly to elliptic flow, which is a global feature of the system, we suspected THERMINATOR 2 could also, at least qualitatively, describe our backgrounds. After ensuring each simulated event received a random event-plane angle (Ψ_{EP})¹, we found THERMINATOR 2 did a good job of describing our data qualitatively, and, in many cases, quantitatively. Figure 11 shows the THERMINATOR 2 simulation (gold) together with experimental data (red, blue, or black). The figure also shows a 6th-order polynomial fit to the simulation (gold), as well as the fit polynomial scaled to match the data (red, blue, black).

Figure 12 shows three different correlation function generated using THERMINATOR 2 simulation (“Cf w/o Bgd (A)”, “Cf w. Bgd (B)”, “Bgd(C)”), as well as two histograms describing the relation between the three (“Ratio (B/C)”, “1+Diff(B-C)”). “Cf w/o Bgd (A)” shows a correlation function with a femtoscopic correlation, but without background. When THERMINATOR 2 is run without randomizing event planes, and therefore having all events share a common event plane, no background is observed, as expected. The femtoscopic correlation effect was introduced by assuming a set of scattering parameters for the system, and weighting the numerators appropriately. The second correlation, ”Cf w. Bgd (B)”, shows a correlation function with both a femtoscopic correlation and a background (most closely matches our situation in experiment). To generate the background, each event was given a random event-plane angle, as is given to us in experiment. To generate the femtoscopic correlation, the same numerator weighting procedure was used. Finally, ”Bgd (C)”, shows a correlation function with a non-femtoscopic background, but no femtoscopic correlation, i.e. background only. This is generated just as ”Cf w. Bgd (B)”, with randomized event planes, but unit weights are used when filling the numerators, so no femtoscopic effects are included.

¹default was for all events to share a common event plane

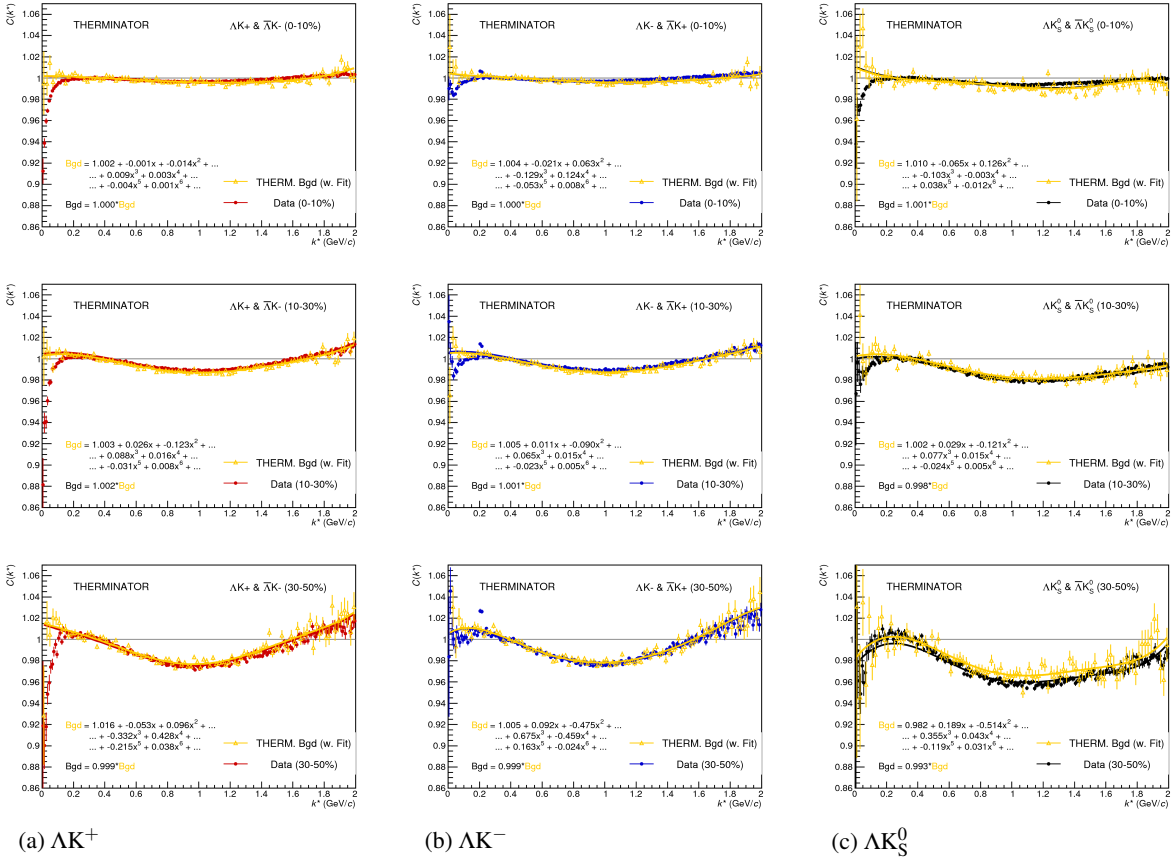


Fig. 11: THERMINATOR 2 simulation (gold) together with experimental data (red, blue, or black). The left column shows results for ΛK^+ (11a), middle for ΛK^- (11b), and right for ΛK_S^0 (11c). A 6th-order polynomial fit to the simulation is shown as a solid gold line, and whose fit parameters are printed on the lower left of each plot. This polynomial is scaled to match the experimental data; the value of this scale is printed in the lower left corner of each plot. The polynomial fit with scale factor applied is drawn in a color matching the experimental data (red, blue, black).

The main point of Fig. 12 is that the black points match the blue (and purple) points; or, equivalently:

$$C_{fw/oBgd} = \frac{C_{fw.Bgd}}{Bgd} \rightarrow C_{theory} = \frac{C_{exp}}{F_{Bgd}} \rightarrow C_{exp} = C_{theory} \cdot F_{Bgd} \quad (17)$$

As shown and described in Fig 12 and Eq. 17, THERMINATOR 2 simulation shows the non-femtoscopic background affects the correlation function as a separable scale factor. We expect this behavior to be roughly the same in the experimental data.

Figure 13 demonstrates the use of the Stavinsky method with THERMINATOR 2. In the figure, unit weights were used for all numerators, so no femtoscopic signal is included, only background effects. The black points show an ideal, experimentally unreachable, situation of aligning all of the event-plane angles. With THERMINATOR 2, when the event-planes are aligned, the background signal is killed. The green points show the case of random event-plane angles, a situation more closely matching that of experiment. The purple points show the affect of applying the Stavinsky method to the case of random event-planes. The figure shows that this method effectively kills the non-flat background (i.e. the procedure takes the green points to the purple). Finally, the blue points show the effect of applying the Stavinsky method when all of the event-planes are aligned. This shows that the Stavinsky method

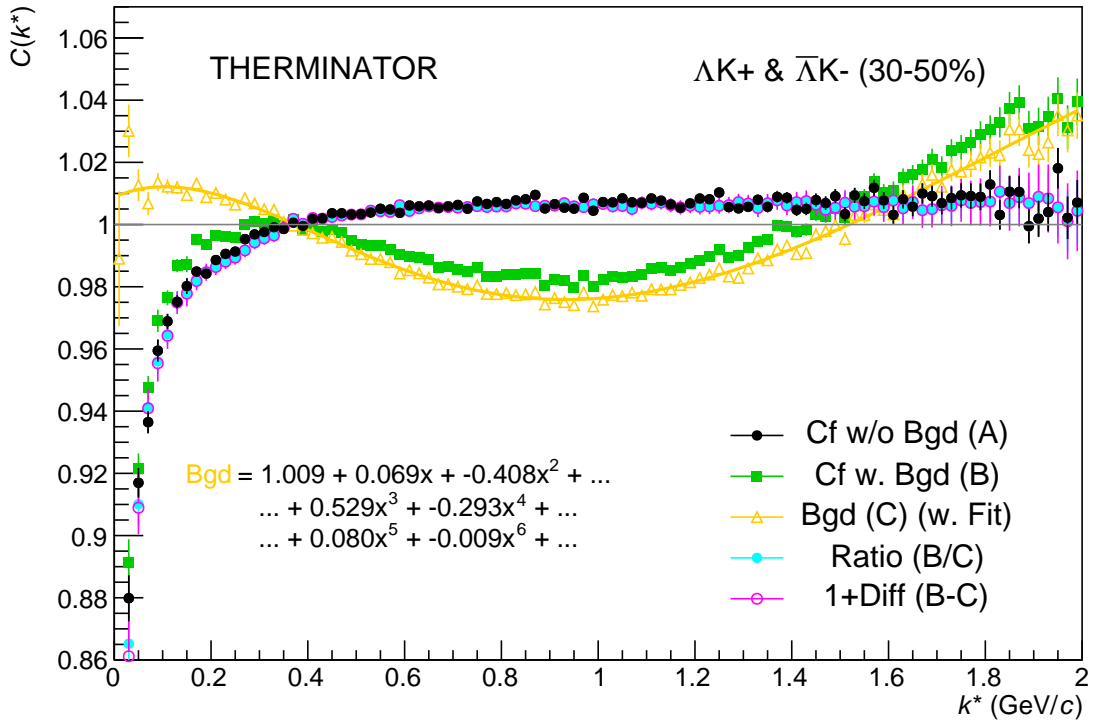


Fig. 12: Correlation with background decomposition with THERMINATOR. "Cf w/o Bgd (A)" shows a correlation function with a femtoscopic correlation, but without background. "Cf w. Bgd (B)", shows a correlation function with both a femtoscopic correlation and a background (most closely matches our situation in experiment). "Bgd (C)", shows a correlation function with a non-femtoscopic background, but no femtoscopic correlation, i.e. background only.

does not introduce any signal to an already flat background.

1.6 LednickyFitter

The code developed to fit the data is called "LednickyFitter", and utilizes the ROOT TMinuit implementation of the MINUIT fitting package. In short, given a function with a number of parameters, the fitter explores the parameter space searching for the minimum of the function. In this implementation, the function to be minimized should represent the difference between the measured and theoretical correlation functions. However, a simple χ^2 test is inappropriate for fitting correlation functions, as the ratio of two Poisson distributions does not result in a Poisson distribution. Instead, a log-likelihood fit function of the following form is used [?]:

$$\chi_{PML}^2 = -2 \left[A \ln \left(\frac{C(A+B)}{A(C+1)} \right) + B \ln \left(\frac{A+B}{B(C+1)} \right) \right] \quad (18)$$

where A is the experimental signal distribution (numerator), B is the experimental background distribution (denominator), and C is the theoretical fit correlation function.

The LednickyFitter uses Equations 2 – 4 to build the theoretical fit, and Equation 18 as the statistic quantifying the quality of the fit. The parameters to be varied by MINUIT are: λ , R , f_0 ($\mathbb{R}f_0$ and $\mathbb{I}f_0$ separately), d_0 , and normalization N . The fitter currently includes methods to correct for momentum resolution and a non-flat background. These corrections are applied to the fit function, the data is never

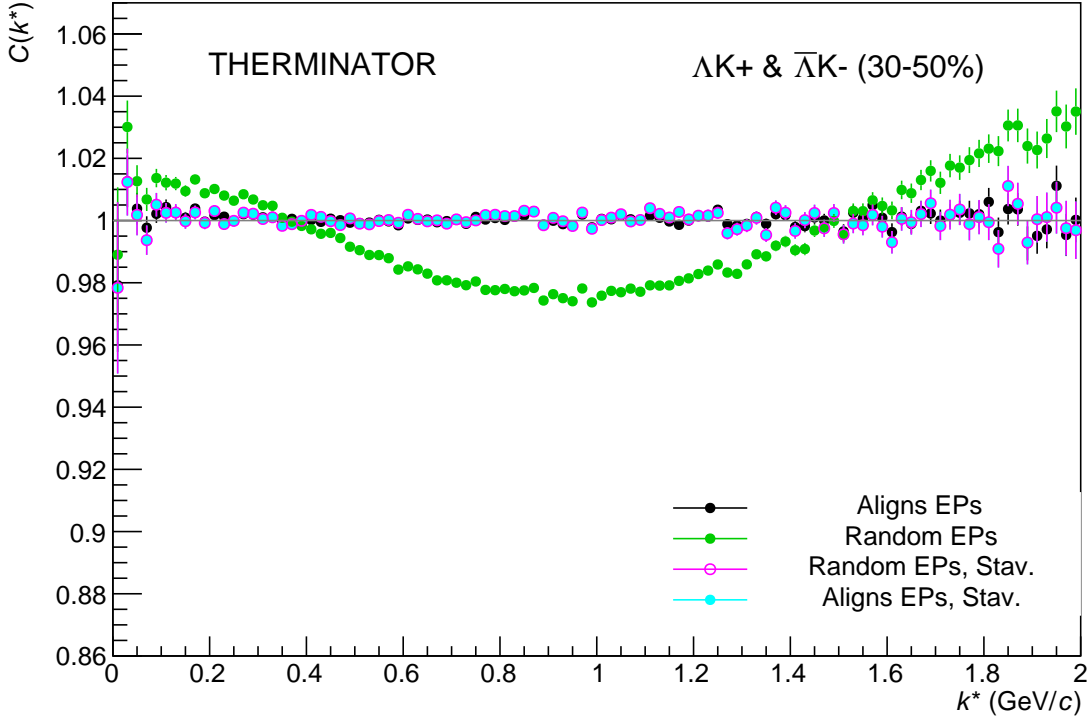


Fig. 13: The use of the Stavinsky method with THERMINATOR 2. Unit weights were used for all numerators, so no femtoscopic signal is included, only background effects. The black points show an ideal, experimentally unreachable, situation of aligning all of the event-plane angles. The green points show the experimental situation of random event-plane angles. The purple points show the affect of applying the Stavinsky method to the case of random event-planes. Finally, the blue points show the effect of applying the Stavinsky method when all of the event-planes are aligned.

touched. The fitter is able to share parameters between different analyses and fit all simultaneously.

In a typical fit, a given pair is fit with its conjugate (ex. ΛK^+ with $\bar{\Lambda} K^-$) across all centralities (0-10%, 10-30%, 30-50%), for a total of 6 simultaneous analyses. Each analysis has a unique λ and normalization parameter. The radii are shared between analyses of like centrality, as these should have similar source sizes. The scattering parameters ($\mathbb{R}f_0$, $\mathbb{I}f_0$, d_0) are shared amongst all.

Initially, we left open the possibility for the $\Lambda K^+(\bar{\Lambda} K^-)$ and $\Lambda K^-(\bar{\Lambda} K^+)$ systems to have different source radii. After always finding these two to be consistent, we decided to join the radii parameters between these systems. So, now, in a typical fit of our ΛK^\pm data, all ΛK^\pm analyses (ΛK^+ , $\bar{\Lambda} K^-$, ΛK^- , $\bar{\Lambda} K^+$) are fit simultaneously across all centralities. Scattering parameters are shared between pair-conjugate systems (i.e. a parameter set describing the ΛK^+ & $\bar{\Lambda} K^-$ system, and a separate set describing the ΛK^- & $\bar{\Lambda} K^+$ system). For each centrality, a radius and λ parameters are shared amongst all pairs. Each analysis has a unique normalization parameter.

In the case of fitting with residuals, the λ_{Fit} parameter serves as an overall normalization shared by all contributors, such that Eqn 14 becomes:

$$\begin{aligned}
C_{measured}(k_{\Lambda K}^*) &= 1 + \sum_i \lambda'_i [C_i(k_{\Lambda K}^*) - 1] \\
\lambda'_i &= \lambda_{Fit} \lambda_i \\
\sum_i \lambda'_i &= \lambda_{Fit} \sum_i \lambda_i = \lambda_{Fit}
\end{aligned} \tag{19}$$

where λ_i is obtained from THERMINATOR, as explained in Section 1.4, and whose values are presented in Tables ?? through ???. For Coulomb-neutral pairs, such as ΛK , $\Sigma^0 K$, and $\Xi^0 K$, $C_i(k_{\Lambda K}^*)$ is calculated from Eqn. 2, with the help of Eqn. 4. For those residual pairs which include a Coulomb interaction, $C_i(k_{\Lambda K}^*)$ is either calculated using the CoulombFitter method (Sections 1.2 and 1.7) with no strong interaction, or by using the $\Xi^{ch} K^{ch}$ data directly. Unless otherwise stated, the $\Xi^{ch} K^{ch}$ residual contribution is modeled using the experimental $\Xi^{ch} K^{ch}$ data, and all other charged contributors (ex. $\Sigma^{*ch} K^{ch}$) are modeled using the CoulombFitter technique with no strong interaction contribution.

To summarize, the complete fit function is constructed as follows:

1. The uncorrected, primary, correlation function, $C_{\Lambda K}(k_{True}^*)$, is constructed using Eq. 19 (with the help of Eqns. 2 and 4)
2. If residuals are included:
 - the parent correlation functions are obtained using:
 - Eq. 19 (with the help of Eqns. 2 and 4) for the case of Coulomb-neutral pairs
 - $\Xi^- K^\pm$ experimental data for $\Xi^- K^\pm$ contributions
 - a Coulomb-only curve, with the help of Secs. 1.2 and 1.7, for pairs including the Coulomb interaction
 - the contribution to the ΛK correlation function is found by running the parent correlation function through the appropriate transform, via Eq.13
3. The primary and residual correlations are combined, via Eq.14, to form $C'_{Fit}(k_{True}^*)$
 - in the case of no residual contributions included in the fit, $\lambda_i = \lambda_{\Lambda K}$ in Eq. 19 is set equal to 1. Then, the extracted λ_{Fit} parameter should be roughly equal to the pair purity
 - when residuals are included, the λ_i values are presented in Table 1
4. The correlation function is corrected to account for momentum resolution effects using Eq. 11

$$- C'_{fit}(k_{Rec}^*) = \frac{\sum_{k_{True}^*} M_{k_{Rec}, k_{True}^*} C'_{fit}(k_{True}^*)}{\sum_{k_{True}^*} M_{k_{Rec}, k_{True}^*}}$$

5. Finally, the non-flat background correction is applied, and the final fit function is obtained

$$- C_{Fit}(k_{Rec}^*) = C'_{Fit}(k_{Rec}^*) * F_{Bgd}(k_{Rec}^*)$$

Figures ??, ??, and ?? (??, ??, and ??, or ??, ??, and ??), in Section ??, show experimental data with fits for all studied centralities for $\Lambda K_S^0 (\bar{\Lambda} K_S^0)$, $\Lambda K^+ (\bar{\Lambda} K^-)$, and $\Lambda K^- (\bar{\Lambda} K^+)$, respectively. In the figures, the black solid line represents the “raw” fit, i.e. not corrected for momentum resolution effects nor non-flat background. The green line shows the fit to the non-flat background. The purple points show the fit after momentum resolution, non-flat background, and residual correlations (if applicable) corrections have been applied. The extracted fit values with uncertainties are also printed on the figures.

1.7 Coulomb Fitter

When fitting the $\Xi^-(\bar{\Xi}^+)K^\pm$ results, it is necessary to include both strong and Coulomb effects. In this case, Equation 2 is no longer valid, and, in fact, there is no analytical form with which to fit. We therefore must take a more basic approach, and integrate out Eq.1 by hand. To achieve this, one has two options. The first option is to numerically integrate Eq.1. The second option is to simulate a large sample of particle pairs, calculate the wave function describing the interaction, and average to obtain the integral. Having no experience with either of these options, we elected the latter of simulating pairs. The code developed to achieve this functionality is called “CoulombFitter”. Currently, in order to generate the statistics needed for a stable fit, we find that $\sim 10^4$ simulated pairs per 10 MeV bin are necessary. The nature of this process means that the “CoulombFitter” takes much longer to run than the “LednickyFitter” of Section 1.1.

Unfortunately, with this analysis, we are not sensitive to, and therefore not able to distinguish between, the iso-spin singlet and triplet states. We proceed with our analysis, but the results must be interpreted as iso-spin averaged scattering parameters.

As stated before, to generate a fit correlation function, we must simulate a large number of pairs, calculate the wave-function, and average Ψ^2 over all pairs in a given k^* bin. Essentially, we calculate Equation 6 by hand:

$$\begin{aligned} C(\mathbf{k}^*) &= \sum_S \rho_S \int S(\mathbf{r}^*) |\Psi_{\mathbf{k}^*}^S(\mathbf{r}^*)|^2 d^3 \mathbf{r}^* \\ &\longrightarrow C(|\mathbf{k}^*|) \equiv C(k^*) = \sum_S \rho_S \langle |\Psi^S(\mathbf{k}_i^*, \mathbf{r}_i^*)|^2 \rangle_i \\ &\longrightarrow C(k^*) = \lambda \sum_S \rho_S \langle |\Psi^S(\mathbf{k}_i^*, \mathbf{r}_i^*)|^2 \rangle_i + (1 - \lambda) \end{aligned} \quad (20)$$

where $\langle \rangle_i$ represents an average over all pairs in a given k^* bin.

In summary, for a given k^* bin, we must draw $N_{pairs} \sim 10^4$ pairs, and for each pair:

1. Draw a random \mathbf{r}^* vector according to our Gaussian source distribution $S(\mathbf{r}^*)$
2. Draw a random \mathbf{k}^* vector satisfying the $|\mathbf{k}^*|$ restriction of the bin
 - We draw from real k^* vectors obtained from the data
 - However, we find that drawing from a distribution flat in k^* gives similar results
3. Construct the wave-function Ψ

After all pairs for a given k^* bin are simulated and wave-functions obtained, the results are averaged to give the fit result.

Construction of the wave-functions, Equation 7, involves a number of complex functions not included in standard C++ or ROOT libraries (namely, $h(\eta)$, $\tilde{G}(\rho, \eta)$), and $F(-i\eta, 1, i\xi)$. These functions were even difficult to find and implement from elsewhere. Our solution was to embed a Mathematica kernel into our C++ code to evaluate these functions. However, having Mathematica work on-the-fly with the fitter was far too time consuming (fitter would have taken days, maybe weeks to finish). Our solution was to use Mathematica to create matrices representing these functions for different parameter values. During fitting, these matrices were then interpolated and the results used to build the wave-functions. This method decreased the running time dramatically, and we are not able to generate results in under ~ 1 hour. This process will be explained in more detail in future versions of the note.